RSC Advances

PAPER

View Article Online
View Journal | View Issue

Cite this: *RSC Adv.*, 2016, **6**, 112226

Stabilization of platinum–nickel alloy nanoparticles with a sulfur-doped graphene support in polymer electrolyte membrane fuel cells†

Calvin Xu, Md Ariful Hoque, Gordon Chiu, Teresa Sung and Zhongwei Chen*

Polymer electrolyte membrane fuel cells (PEMFC) are limited by the sluggish oxygen reduction reaction (ORR) at the cathode, necessitating the use of platinum-based catalysts for practical use. However, such catalysts suffer from degradation issues related to the catalyst and the support material that prevent prolonged operation. Sulfur-doped graphene (SG) as a catalyst support material promises high durability with pure Pt, but its contribution to lattice-strained Pt as in bimetallic alloys has not yet been determined. In this work, platinum–nickel alloy nanoparticles with SG are synthesized (denoted as Pt–Ni/SG), then chemically dealloyed (denoted as Pt–Ni/SG-DA) and finally subjected to a post heat treatment (denoted as Pt–Ni/SG-PHT). The prepared catalysts Pt–Ni/SG, Pt–Ni/SG-DA and Pt–Ni/SG-PHT are physically characterized and electrochemically tested in half-cell conditions. Pt–Ni/SG-PHT is found to be superior, exhibiting the highest ECSA and mass activity retention with losses of 27 and 28% respectively after 1500 cycles from 0.05 to 1.3 V *vs.* RHE in $HClO_4$. This is compared to a 59% ECSA loss and 69% activity loss for commercial Pt/C under the same conditions. Hence, the strong interaction between the metal particles and sulfur-doped graphene resulting from the annealing process as in Pt–Ni/SG-PHT yields a highly stable electrocatalyst for the ORR.

Received 6th August 2016
Accepted 7th November 2016

DOI: 10.1039/c6ra19924k

www.rsc.org/advances

1. Introduction

Continued use of non-renewable fossil fuels is becoming more economically and environmentally unsustainable, leading to an unmet demand for alternative sources of energy generation. Among these new sources, polymer electrolyte membrane fuel cells facilitated by a platinum-group metal catalyzing the oxygen reduction reaction (ORR) at the cathode have attracted much interest as a green power technology. In turn, the practicality of such fuel cells is limited by the scarcity of platinum and the loss of output power after degradation from continued use. Motivated by the high costs of these catalysts, a reduced noble metal loading has been made possible by compensating with high activity electrocatalysts. Approaches to increase catalytic activity include alloying Pt with transition metals and supporting the metal with stable carbon nanomaterials such as carbon nanotubes[1] or graphene.[2,3] It has been reported that the lattice-strain phenomenon is the primary mechanism[4–7] by which platinum alloys can achieve greater catalytic activity over platinum alone. Oxygen binds too strongly to pure platinum due to the latter's d-band electron energy levels[8] but by inducing a strain on the surface through metal alloying, the electronic structure of the surface can be shifted so that oxygen species are bound more weakly, allowing adsorbed OH to more easily dissociate and free the active site.[9] This has been shown with transition metals such as iron,[10–12] copper[13] and cobalt[14–18] as well as with noble metals in nanostructure morphologies.[19–23] In particular, nickel-based alloys have shown levels of catalytic activity greater than those based on other transition metals.[24–29]

Unfortunately, there are major challenges with transition metal dissolution under acidic conditions due to the low dissolution potentials of such elements. In addition, other concerns with the stability of PEMFC catalysts involve the degradation of the support material, which is typically carbon black. This results in either the breakoff of attached metal particles from the support or the direct corrosion of the carbon itself, both of which are exacerbated at upper operating potentials.[30,31] As this is the result of weak interaction between the support and active material, dissolution and support instability can be solved either by robust Pt morphologies or through enhanced bonding between the electrocatalyst components.[33–35] Nanocarbon support materials such as graphene have become increasingly popular as the main focus of catalytic research in recent years. Furthermore, doping graphene with elements such as nitrogen,[36] phosphorus and boron has yielded improved catalytic performance.[37–39] In particular, recent developments involving sulfur have yielded impressive platinum-based catalysts.[40–42] This doping technique has further been observed to

Department of Chemical Engineering, Waterloo Institute for Nanotechnology, Waterloo Institute of Sustainable Energy, University of Waterloo, 200 University Ave. W, Waterloo, ON, N2L 3G1, Canada. E-mail: zhwchen@uwaterloo.ca

† Electronic supplementary information (ESI) available. See DOI: 10.1039/c6ra19924k

improve the longevity of the catalyst,[43] and this is posited as due to the strengthened metal-support bond preventing the breakoff of the metal species.[44] As such, the incorporation of sulfur-doped graphene (SG) as in this work would show great promise for improving the activity and stability of Pt alloy catalysts.

Previously, our group had reported the use of SG to support platinum nanoparticles and nanowires with the effect of increased activity and stability, with density functional theory (DFT) modelling corroborating these results.[39,41,43] In these simulations, it was determined that pure platinum deposited onto sulfur-doped graphene (Pt/SG) had an adsorption energy of −2.68 eV *versus* −2.01 eV for pure platinum on graphene (Pt/G), a d-band centre at −2.72 eV for Pt/SG *versus* −2.33 eV for Pt/G, and a cohesive energy of −3.95 eV for Pt/SG *versus* −3.67 eV for Pt/G. However, the synergistic behaviour between SG and alloyed platinum has yet to be investigated. The changes in electronic structure introduced into a Pt alloy by the lattice-strain from a transition metal such as nickel can have very drastic effects on the binding strengths of sulfur dopants as compared to pure Pt, and the impact on both catalytic activity as well as stability must be considered. Herein, we report the performance of a platinum–nickel catalyst supported by SG, here referred to as Pt–Ni/SG, and the role of SG for bimetallic Pt–Ni. The synthesis of the alloy was conducted using the well-established polyol method as found in literature, then the catalyst was chemically dealloyed for Pt–Ni/SG-DA and finally subjected to thermal annealing for Pt–Ni/SG-PHT. Electrochemical testing was performed on the alloy, dealloyed and heat treated catalysts with physical characterization used to correlate the behaviour with the catalyst morphology with the final as-prepared catalyst Pt–Ni/SG-PHT demonstrating excellent stability as compared to commercial Pt/C.

2. Experimental

Physico-chemical characterization

Samples were imaged by transmission electron microscope (TEM, JEOL 2010F). Characterization was also conducted through X-ray diffraction (XRD, Rigaku Miniflex), and inductively coupled plasma spectroscopy (ICP, Teledyne Leeman Labs Prodigy High Dispersion ICP system).

Electrochemical measurements

For electrochemical testing, a five-neck glass cell for rotating electrodes was filled with 200 mL 0.1 M $HClO_4$, with a Pt wire as the counter-electrode and a reversible hydrogen electrode (RHE) as the reference electrode. A 0.196 cm^2 glassy carbon working electrode was cleaned and polished thoroughly prior to deposition with 10 μL of catalyst ink (2 mg of catalyst dispersed in 990 μL of 1-propanol and 10 μL of 5 wt% Nafion® solution). All working electrodes were prepared with a Pt loading of 20 μg cm^{-2}, and the ink composition of the commercial Pt/C (TKK, 28 wt% Pt) used in comparison was modified accordingly. Each catalyst was electrochemically activated in N_2-saturation by cycling from 0.05 to 1.3 V *vs.* RHE at a scan rate of 50 mV s^{-1} for 30 cycles to obtain the steady-state cyclic voltammogram (CV) curve. The electrochemical surface area (ECSA), in $m^2\ g^{-1}$, was determined *via* the equation:

$$\mathrm{ECSA} = \frac{Q/r}{\Gamma \times L \times A}$$

where Q, in coulombs, corresponds to the charge integrated from the hydrogen desorption peak from the anodic sweep; r is the scan rate in mV s^{-1}, $\Gamma = 210$ μC cm^{-2} is the charge required to reduce a hydrogen monolayer from a polycrystalline Pt surface; L is the Pt loading onto the glassy carbon working electrode, here taken to be 20 μg cm^{-2}; and A is the area of the glassy carbon electrode in cm^2.[45–48] Accelerated durability testing (ADT) was conducted in similar conditions, with 1500 cycles from 0.05 to 1.3 V *vs.* RHE instead. The CV of each catalyst was obtained pre- and post-ADT. Pre- and post-ADT ORR polarization curves were obtained from the anodic scan from 0.05 to 1.2 V *vs.* RHE at 5 mV s^{-1} in O_2-saturation.

Graphene oxide (GO) synthesis

Graphite was oxidized *via* an improved Hummer's method to yield GO as described in literature.[41] Briefly, 2 g of graphite powder (Alfa Aesar, natural, microcrystal grade, APS 2–15 micron, 99.9995%) was added to a mixture of concentrated H_2SO_4/H_3PO_4 (360 : 40 mL) in an Erlenmeyer flask and stirred for 30 minutes. 18 g of $KMnO_4$ was then added very slowly to the mixture, and the flask was heated to 50 °C for 16 hours. After heating, the flask was cooled to approximately 10 °C in an ice bath and 400 mL of DDI H_2O was added to the mixture dropwise. Finally, 15 mL of H_2O_2 (30%) was added to the mixture. The mixture was centrifuged and washed with water, ethanol and HCl (30%), and then freeze dried for 3–4 days.

Sulfur-doped graphene (SG) synthesis

GO was mixed with phenyl disulfide (99%, Sigma-Aldrich) in a 2 : 1 weight ratio and ground together into a fine powder using a mortar and pestle. Using a tube furnace, the powder was then annealed at 1000 °C for 30 minutes at a 20 °C min^{-1} ramp rate with argon flowing at 100 sccm.

Synthesis of SG supported Pt–Ni nanoparticles

Deposition of platinum nanoparticles onto SG was achieved *via* ethylene glycol and the polyol process,[49] and this catalyst is denoted as Pt/SG. The Pt–Ni/SG alloy was synthesized by annealing the Pt/SG with nickel(II) nitrate hexahydrate in a 1 : 3 Pt–Ni molar ratio at 600 °C for 7 h in a 100 sccm flow rate of 10% H_2–Ar and 10 °C min^{-1} heating rate. The Pt–Ni/SG was chemically dealloyed with 0.5 M sulphuric acid at 80 °C for 24 hours, denoted as Pt–Ni/SG-DA. Post heat treatment of the Pt–Ni/SG-DA was performed at 400 °C for 1 hour in similar conditions as above, denoted as Pt–Ni/SG-PHT.

3. Results and discussion

Physico-chemical characterization

TEM images of the samples Pt–Ni/SG, Pt–Ni/SG-DA and Pt–Ni/SG-PHT reveal the morphology of the electrocatalyst as

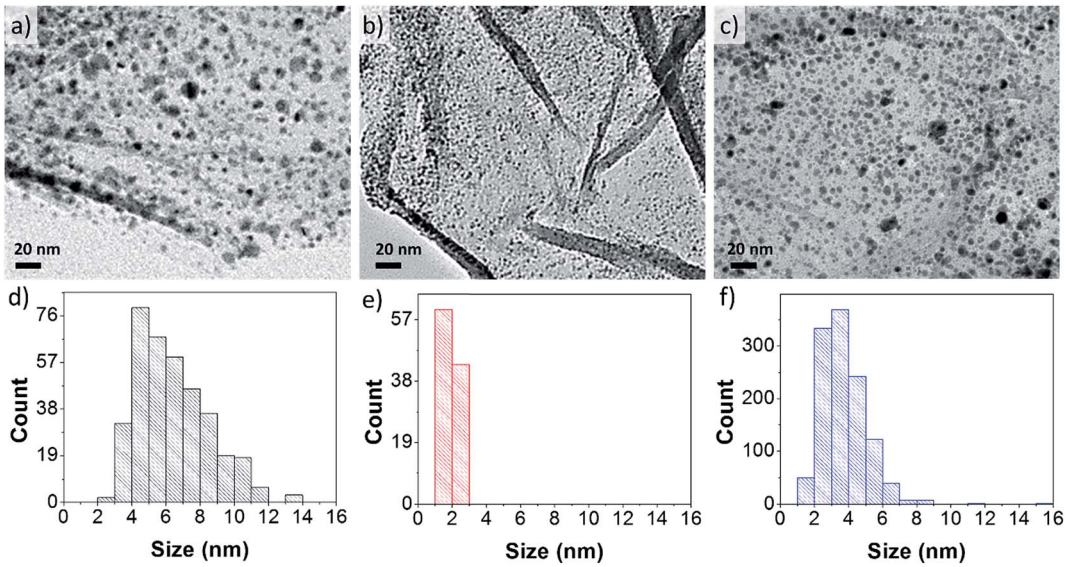

Fig. 1 TEM imaging of the (a) Pt–Ni/SG, (b) Pt–Ni/SG-DA and (c) Pt–Ni/SG-PHT electrocatalysts. Particle size distributions of these catalysts are shown below the respective microscopy images, with (d) Pt–Ni/SG, (e) Pt–Ni/SG-DA and (f) Pt–Ni/SG-PHT.

subsequent preparation techniques are performed. These images can be seen progressively in Fig. 1(a–c) with the associated particle size distributions shown in Fig. 1(d–f). The morphology of SG itself is shown through SEM in Fig. S1(a) (ESI†), and the presence of sulfur in the sheets is confirmed in Fig. S1(b) (ESI†). It can be observed that the freshly prepared Pt–Ni/SG has a comparably broader particle size distribution than that of the others and this is due to the high temperature at which annealing was performed. Compared to the alloy particles with a wide distribution from 3–10 nm, the dealloyed nanoparticles of Pt–Ni/SG-DA are noted to be diminished to a monodisperse diameter of approximately 2 nm. This size reduction is the result of transition metal leaching from the particles, leaving platinum as the dominant species. This concurs with literature findings where particles of this size were noted to be etched to smaller diameters after dealloying rather than form nanoporous particles of the same size.[50,51] Following a second heat treatment of the dealloyed sample for the Pt–Ni/SG-PHT catalyst, it can be seen from the size distribution that such a treatment has again stimulated a growth in particle size and a broadening of the distribution to 2–7 nm. However, the mean particle size as well as the spread in diameter is smaller than that of the alloyed particles as the post-heat treatment was

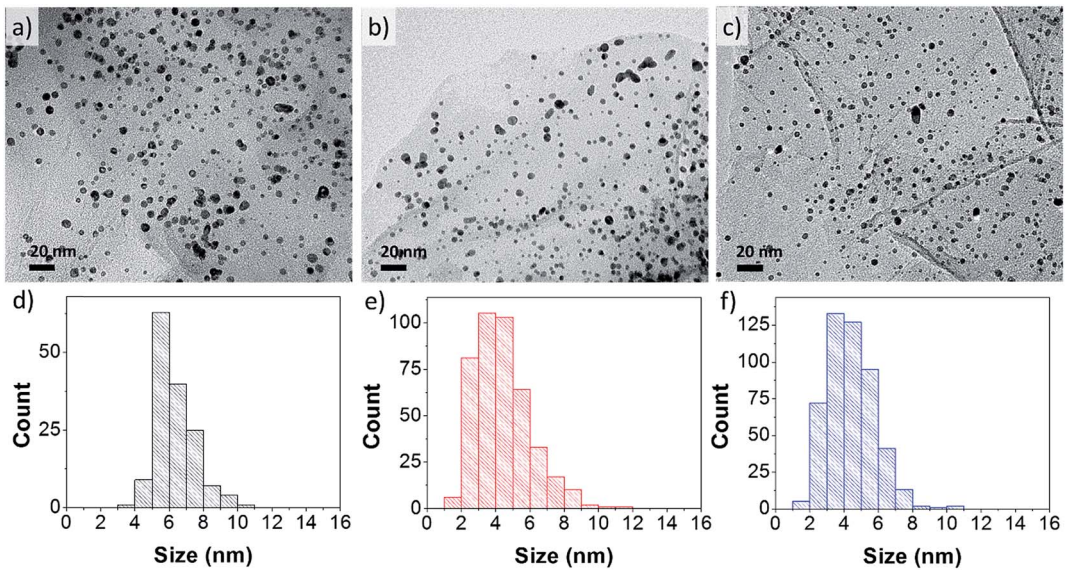

Fig. 2 TEM imaging of the (a) Pt–Ni/SG-ADT, (b) Pt–Ni/SG-DA-ADT and (c) Pt–Ni/SG-PHT-ADT electrocatalysts. Particle size distributions of these catalysts are shown below the respective microscopy images, with (d) Pt–Ni/SG-ADT, (e) Pt–Ni/SG-DA-ADT and (f) Pt–Ni/SG-PHT-ADT.

not as great in temperature or exposure time as the first treatment step.

The morphologies of the catalysts after ADT can be seen in Fig. 2(a–c), and their corresponding size distributions are shown in Fig. 2(d–f). From the particle size distributions of the three catalysts, it is clear that ADT has the effect of increasing the size of the metal particles. This observation concurs with well-known mechanisms of catalyst degradation such as migration of platinum and Ostwald ripening.[32] The size increase is most prevalent in Pt–Ni/SG, with the small <4 nm particles absent in Pt–Ni/SG-ADT. The maximum size of the Pt–Ni/SG-DA particles increases to 8 nm after ADT, and it is obvious that the size monodispersity of 2 nm is lost. It is interesting to note that the distributions of Pt–Ni/SG-PHT and Pt–Ni/SG-PHT-ADT differ very little, indicating the stability of this catalyst. Following the annealing step, the catalyst becomes very resistant to further changes in the size of the particles and the durability of Pt–Ni/SG-PHT is noted to be the greatest. On the other hand, the particle growth rate of Pt/C, shown in Fig. S2 (ESI†), is much more pronounced than that of Pt–Ni/SG-PHT. Through ICP analysis, the metal content was determined for each of the freshly synthesized catalysts. From Table S1 (ESI†), it can be seen that a platinum loading of approximately 10 wt% was achieved. After chemical dealloying, nickel leached from the particles and the absence of the metal after characterization is expected. There is also a minute loss in platinum from this technique. After post-heat treatment, extant functional groups such as –OH moieties are removed from the graphene support and hence, an increase in both nickel and platinum content can be seen. From the XRD spectra of the catalysts in Fig. S3 (ESI†), the peaks in Pt–Ni/SG indicates the presence of Ni particles during synthesis of the platinum–nickel alloy. However, after the leaching of nickel by dealloying for Pt–Ni/SG-DA and post-heat treatment for Pt–Ni/SG-PHT, well defined peaks related to Pt (111) can be observed. A qualitative visualization of the composition changes can be seen *via* elemental mapping in Fig. S5 to S10 (ESI†).

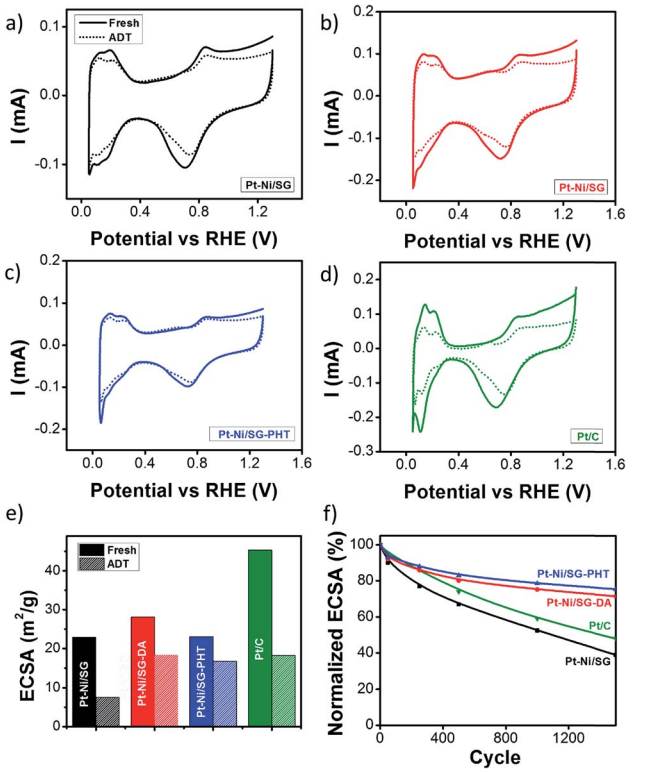

Fig. 3 CV at 50 mV s^{-1} in N_2-saturated 0.1 M $HClO_4$, before and after ADT of 1500 cycles from 0.05 to 1.3 V, for (a) alloyed Pt–Ni/SG, (b) dealloyed Pt–Ni/SG-DA, (c) post-heat treated Pt–Ni/SG-PHT and (d) commercial Pt/C using a 0.196 cm^2 glassy carbon working electrode and Pt wire counter electrode. Catalyst stability comparison through (e) absolute ECSA and (f) normalized ECSA as a function of potential cycling.

Electrochemical characterization

Pre- and post-ADT CVs from 0.05 to 1.3 V *vs.* RHE for the as-prepared catalysts Pt–Ni/SG, Pt–Ni/SG-DA and Pt–Ni/SG-PHT as well as the commercial Pt/C are shown in Fig. 3(a–d). The pre- and post-ADT ECSA as shown in Fig. 3(e) were respectively 23.0 and 7.6 $m^2\ g^{-1}$ for Pt–Ni/SG, 28.1 and 18.4 $m^2\ g^{-1}$ for Pt–Ni/SG-DA, 23.0 and 16.7 $m^2\ g^{-1}$ for Pt–Ni/SG-PHT and 45.3 $m^2\ g^{-1}$ and 18.3 $m^2\ g^{-1}$ for Pt/C. The normalized ECSA of the catalysts can be seen in Fig. 3(f), and the percent loss in ECSA after ADT was 66, 34, 27 and 59% for Pt–Ni/SG-ADT, Pt–Ni/SG-DA-ADT, Pt–Ni/SG-PH-ADT and commercial Pt/C respectively. The increase in ECSA from the alloy to dealloyed catalyst can be correlated with the particle size distributions of the two, with the latter having particles at a relatively monodisperse 2–3 nm diameter. Finally, the thermal treatment of the dealloyed catalyst to form Pt–Ni/SG-PHT lead not only to particle size growth but also a correlated decrease in ECSA similar to that of the alloy catalyst. The ECSA change following ADT clearly shows the greater stability of Pt–Ni/SG-PHT, and this retention can be attributed to the metal particle stabilization to SG following post-heat treatment. Thus, the benefits of SG lie in the strong interactions created between Pt and SG.

The ORR polarization curves of the catalysts can be seen in Fig. 4(a–d). From the limiting current in each catalyst, the mass-transport corrected kinetic current was derived to obtain the respective mass activities. The change in half-wave potentials for Pt–Ni/SG, Pt–Ni/SG-DA and Pt–Ni/SG-PHT were 38.7, 32.2 and 8.4 mV respectively, compared to 46.8 mV for Pt/C. The initial mass activity calculated at 0.9 V *vs.* RHE of Pt–Ni/SG, Pt–Ni/SG-DA, Pt–Ni/SG-PHT, and Pt/C was 190, 153, 93 and 125 mA mg_{Pt}^{-1} respectively, while the mass activity after ADT was 42, 55, 67, and 39 mA mg_{Pt}^{-1} respectively, shown in Fig. 4(e). This means that mass activity loss is respectively 77.9, 64.1, 28.0 and 68.8%. Similarly, the specific activities at 0.9 V *vs.* RHE of Pt–Ni/SG, Pt–Ni/SG-DA, and Pt–Ni/SG-PHT were 829, 544, and 405 μA cm_{Pt}^{-2} respectively which were higher than that of Pt/C at 266 μA cm_{Pt}^{-2}. The specific activities of these catalysts from 0.85 to 0.95 V *vs.* RHE are displayed in Fig. 4(f). The platinum content in the alloy catalyst as determined *via* ICP analysis was relatively low due to the dominance of nickel in the metal content, and this deficiency is expected to be a major factor in its limited activity improvement over Pt/C. The poor stability of Pt–Ni/SG

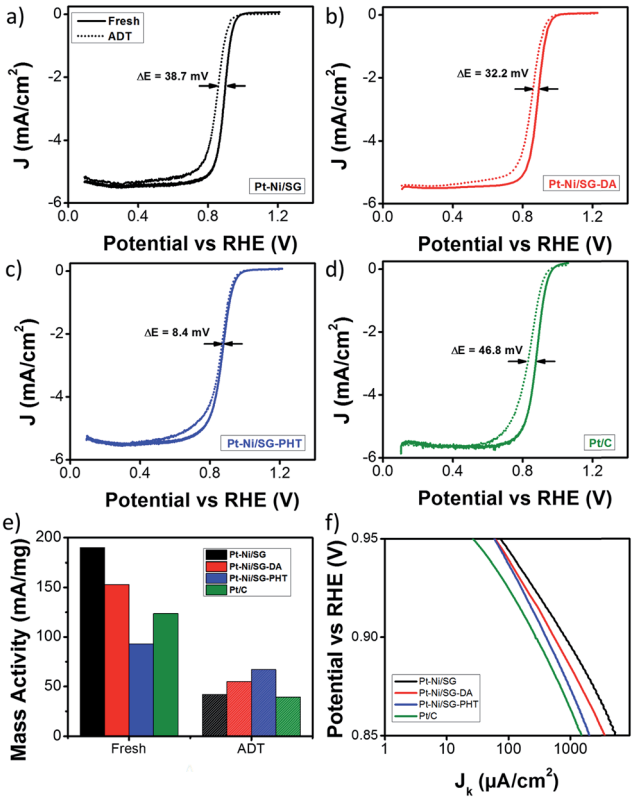

Fig. 4 ORR polarization curves at 5 mV s^{-1} in O_2-saturated 0.1 M $HClO_4$, before and after ADT of 1500 cycles from 0.05 to 1.3 V, for (a) alloyed Pt–Ni/SG, (b) dealloyed Pt–Ni/SG-DA, (c) post-heat treated Pt–Ni/SG-PHT and (d) commercial TKK Pt/C (28.2 wt% Pt) using a 0.196 cm^2 glassy carbon working electrode and Pt wire counter electrode. The prepared catalysts are compared to commercial Pt/C through (e) mass activity change before and after ADT, and (f) specific activities from 0.85 to 0.95 V.

with respect to mass activity is attributed to dissolution of the transition metal under the electrochemical conditions as indicated by Pourbaix diagrams,[52] which is to be compared to the greater resilience in more noble metals such as Pd.[53,54] After chemically-induced nickel leaching to form the Pt–Ni/SG-DA, there is a decrease in mass activity as compared to the alloy due to the loss of favourable phenomena provided by the transition metal including strain and ligand effects. Despite a lower initial mass activity than the alloy, the dealloyed catalyst suffered from a smaller activity loss as there was no significant nickel present for dissolution to occur from the nanoparticles. The increase in particle size for Pt–Ni/SG-PHT finally yields the lowest activity of the three electrocatalysts, but the thermal exposure also resulted in the highest interaction between the particles and catalyst support. As such, it has the highest stability and its loss in activity is the smallest of all. Overall, the increased durability of Pt–Ni/SG-PHT over Pt/C can be attributed to the thiophenic sulfur moieties in the support material, which has previously been observed to be the source of strong binding between Pt and the doped graphene due to electronic structure modifications and strong catalyst–support interactions.[41–43] Such thiophene-like sulfur has also been previously identified experimentally through XPS spectra of SG used as a Pt-free catalyst,[55] though prior conclusions with regards to stability can only be inferred as the sulfur–carbon bonds preventing carbon corrosion upon which Pt nucleation sites reside.[56]

4. Conclusion

In summary, platinum–nickel alloy nanoparticles supported by SG were prepared and the physico-chemical as well as electrochemical characterization as per half-cell conditions was performed. This was done for the catalyst in its alloyed, dealloyed, and post-heat treated form with Pt–Ni/SG-PHT being found to have superior stability as it has the greatest retention in both ECSA and mass activity, with only a 27% loss in the former and a 28% loss in the latter. This is compared to a 59% ECSA loss and 69% activity loss for commercial Pt/C. The exceptional stability of Pt–Ni/SG-PHT demonstrates the Pt–SG interaction effects from sulfur doping to provide a highly durable catalyst support for the PEMFC cathode.

Acknowledgements

The authors are grateful for financial support provided by the Natural Sciences and Engineering Research Council of Canada (NSERC), the University of Waterloo and the Waterloo Institute for Nanotechnology, as well as TEM imaging provided by the Canadian Center for Electron Microscopy (CCEM).

References

1 D. C. Higgins, D. Meza and Z. Chen, *J. Phys. Chem. C*, 2010, **114**, 21982–21988.
2 D. Higgins, P. Zamani, A. Yu and Z. Chen, *Energy Environ. Sci.*, 2016, **9**, 357–390.
3 B. Y. Xia, H. Bin Wu, Y. Yan, H. B. Wang and X. Wang, *Small*, 2014, **10**, 2336–2339.
4 P. Strasser, S. Koh, T. Anniyev, J. Greeley, K. More, C. Yu, Z. Liu, S. Kaya, D. Nordlund, H. Ogasawara, M. F. Toney and A. Nilsson, *Nat. Chem.*, 2010, **2**, 454–460.
5 M. Shao, J. H. Odell, A. Peles and D. Su, *Chem. Commun.*, 2014, **50**, 2173–2176.
6 V. A. Sethuraman, D. Vairavapandian, M. C. Lafouresse, T. A. Maark, N. Karan, S. Sun, U. Bertocci, A. A. Peterson, G. R. Stafford and P. R. Guduru, *J. Phys. Chem. C*, 2015, **119**, 19042–19052.
7 S. Zhang, X. Zhang, G. Jiang, H. Zhu, S. Guo, D. Su, G. Lu and S. Sun, *J. Am. Chem. Soc.*, 2014, **136**, 7734–7739.
8 J. K. Nørskov, J. Rossmeisl, A. Logadottir, L. Lindqvist, J. R. Kitchin, T. Bligaard and H. Jónsson, *J. Phys. Chem. B*, 2004, **108**, 17886–17892.
9 V. Stamenkovic, B. S. Mun, K. J. J. Mayrhofer, P. N. Ross, N. M. Markovic, J. Rossmeisl, J. Greeley and J. K. Nørskov, *Angew. Chem., Int. Ed.*, 2006, **45**, 2897–2901.
10 S. Guo and S. Sun, *J. Am. Chem. Soc.*, 2012, **134**, 2492–2495.
11 H. Zhu, S. Zhang, D. Su, G. Jiang and S. Sun, *Small*, 2015, **11**, 3545–3549.

12 Q. Li, L. Wu, G. Wu, D. Su, H. Lv, S. Zhang, W. Zhu, A. Casimir, H. Zhu, A. Mendoza-Garcia and S. Sun, *Nano Lett.*, 2015, **15**, 2468–2473.
13 X. Sun, D. Li, Y. Ding, W. Zhu, S. Guo, Z. L. Wang and S. Sun, *J. Am. Chem. Soc.*, 2014, **136**, 5745–5749.
14 D. C. Higgins, S. Ye, S. Knights and Z. Chen, *Electrochem. Solid-State Lett.*, 2012, **15**, B83.
15 D. C. Higgins, R. Wang, M. A. Hoque, P. Zamani, S. Abureden and Z. Chen, *Nano Energy*, 2014, **10**, 135–143.
16 I. Spanos, J. J. K. Kirkensgaard, K. Mortensen and M. Arenz, *J. Power Sources*, 2014, **245**, 908–914.
17 B. N. Wanjala, B. Fang, S. Shan, V. Petkov, P. Zhu, R. Loukrakpam, Y. Chen, J. Luo, J. Yin, L. Yang, M. Shao and C. J. Zhong, *Chem. Mater.*, 2012, **24**, 4283–4293.
18 B. Y. Xia, H. Bin Wu, N. Li, Y. Yan, X. W. D. Lou and X. Wang, *Angew. Chem., Int. Ed.*, 2015, **54**, 3797–3801.
19 A. Peles, M. Shao and L. Protsailo, *Catalysts*, 2015, **5**, 1193–1201.
20 S. Il Choi, M. Shao, N. Lu, A. Ruditskiy, H. C. Peng, J. Park, S. Guerrero, J. Wang, M. J. Kim and Y. Xia, *ACS Nano*, 2014, **8**, 10363–10371.
21 M. Shao, A. Peles and J. Odell, *J. Phys. Chem. C*, 2014, **118**, 18505–18509.
22 M. Shao, G. He, A. Peles, J. H. Odell, J. Zeng, D. Su, J. Tao, T. Yu, Y. Zhu and Y. Xia, *Chem. Commun.*, 2013, **49**, 9030–9032.
23 M. P. Humbert, B. H. Smith, Q. Wang, S. N. Ehrlich and M. Shao, *Electrocatalysis*, 2012, **3**, 298–303.
24 V. R. Stamenkovic, B. Fowler, B. S. Mun, G. Wang, P. N. Ross, C. A. Lucas and N. M. Marković, *Science*, 2007, **315**, 493–497.
25 D. F. van der Vliet, C. Wang, D. Tripkovic, D. Strmcnik, X. F. Zhang, M. K. Debe, R. T. Atanasoski, N. M. Markovic and V. R. Stamenkovic, *Nat. Mater.*, 2012, **11**, 1051–1058.
26 C. Cui, L. Gan, H. H. Li, S. H. Yu, M. Heggen and P. Strasser, *Nano Lett.*, 2012, **12**, 5885–5889.
27 S. Il Choi, S. Xie, M. Shao, J. H. Odell, N. Lu, H. C. Peng, L. Protsailo, S. Guerrero, J. Park, X. Xia, J. Wang, M. J. Kim and Y. Xia, *Nano Lett.*, 2013, **13**, 3420–3425.
28 S. Il Choi, S. Xie, M. Shao, N. Lu, S. Guerrero, J. H. Odell, J. Park, J. Wang, M. J. Kim and Y. Xia, *ChemSusChem*, 2014, **7**, 1476–1483.
29 S. Zhang, Y. Hao, D. Su, V. V. T. Doan-Nguyen, Y. Wu, J. Li, S. Sun and C. B. Murray, *J. Am. Chem. Soc.*, 2014, **136**, 15921–15924.
30 M. A. Hoque, D. C. Higgins, F. M. Hassan, J.-Y. Choi, M. D. Pritzker and Z. Chen, *Electrochim. Acta*, 2014, **121**, 421–427.
31 S. Y. Huang, P. Ganesan, S. Park and B. N. Popov, *J. Am. Chem. Soc.*, 2009, **131**, 13898–13899.
32 Z. Chen, M. Waje, W. Li and Y. Yan, *Angew. Chem., Int. Ed.*, 2007, **46**, 4060–4063.
33 B. Y. Xia, H. Bin Wu, X. Wang and X. W. Lou, *Angew. Chem., Int. Ed.*, 2013, **52**, 12337–12340.
34 B. Y. Xia, H. Bin Wu, Y. Yan, X. W. Lou and X. Wang, *J. Am. Chem. Soc.*, 2013, **135**, 9480–9485.
35 B. Y. Xia, W. T. Ng, H. Bin Wu, X. Wang and X. W. Lou, *Angew. Chem., Int. Ed.*, 2012, **51**, 7213–7216.
36 J.-Y. Choi, D. U. Lee and Z. Chen, *ECS Trans.*, 2013, **50**, 1815–1822.
37 N. Cheng, J. Liu, M. N. Banis, D. Geng, R. Li, S. Ye, S. Knights and X. Sun, *Int. J. Hydrogen Energy*, 2014, **39**, 15967–15974.
38 H. N. Yang, D. C. Lee, K. W. Park and W. J. Kim, *Energy*, 2015, **89**, 500–510.
39 D. C. Higgins, F. M. Hassan, M. H. Seo, J. Y. Choi, M. A. Hoque, D. U. Lee and Z. Chen, *J. Mater. Chem. A*, 2015, **3**, 6340–6350.
40 R. Wang, D. C. Higgins, M. A. Hoque, D. Lee, F. Hassan and Z. Chen, *Sci. Rep.*, 2013, **3**, 2431.
41 M. A. Hoque, F. M. Hassan, M.-H. Seo, J.-Y. Choi, M. Pritzker, S. Knights, S. Ye and Z. Chen, *Nano Energy*, 2016, **19**, 27–38.
42 M. A. Hoque, F. M. Hassan, D. Higgins, J. Y. Choi, M. Pritzker, S. Knights, S. Ye and Z. Chen, *Adv. Mater.*, 2015, **27**, 1229–1234.
43 D. Higgins, M. A. Hoque, M. H. Seo, R. Wang, F. Hassan, J.-Y. Choi, M. Pritzker, A. Yu, J. Zhang and Z. Chen, *Adv. Funct. Mater.*, 2014, **24**, 4325–4336.
44 Y. Zhou, K. Neyerlin, T. S. Olson, S. Pylypenko, J. Bult, H. N. Dinh, T. Gennett, Z. Shao and R. O'Hayre, *Energy Environ. Sci.*, 2010, **3**, 1437.
45 Y. Garsany, O. A. Baturina, K. E. Swider-Lyons and S. S. Kocha, *Anal. Chem.*, 2010, **82**, 6321–6328.
46 A. Pozio, M. De Francesco, A. Cemmi, F. Cardellini and L. Giorgi, *J. Power Sources*, 2002, **105**, 13–19.
47 K. R. Cooper, *Fuel Cell Mag.*, 2009, 1–3.
48 K. Shinozaki, J. W. Zack, R. M. Richards, B. S. Pivovar and S. S. Kocha, *J. Electrochem. Soc.*, 2015, **162**, F1144–F1158.
49 S. Sharma and B. G. Pollet, *J. Power Sources*, 2012, **208**, 96–119.
50 J. Snyder, I. McCue, K. Livi and J. Erlebacher, *J. Am. Chem. Soc.*, 2012, **134**, 8633–8645.
51 L. Gan, M. Heggen, R. O'Malley, B. Theobald and P. Strasser, *Nano Lett.*, 2013, **13**, 1131–1138.
52 A. Holewinski, J.-C. Idrobo and S. Linic, *Nat. Chem.*, 2014, **6**, 828–834.
53 S. Khateeb, S. Guerreo, D. Su, R. M. Darling, L. V. Protsailo and M. Shao, *J. Electrochem. Soc.*, 2016, **163**, F708–F713.
54 L. Zhang, S. Zhu, Q. Chang, D. Su, J. Yue, Z. Du and M. Shao, *ACS Catal.*, 2016, 3428–3432.
55 L. Zhang, J. Niu, M. Li and Z. Xia, *J. Phys. Chem. C*, 2014, **118**, 3545–3553.
56 J. Liang, Y. Jiao, M. Jaroniec and S. Z. Qiao, *Angew. Chem., Int. Ed.*, 2012, **51**, 11496–11500.